A unified quantum field description of spontaneous and stimulated nonlinear wave mixing and Hyper-Rayleigh scattering

Oleksiy Roslyak & Shaul Mukamel

Department of Chemistry, University of California,
Irvine, CA,92697

January 29, 2010

Abstract

By combining a quantum treatment of the radiation field with a superoperator formalism we derived compact expressions for the various coherent and incoherent nonlinear optical signals. Using molecular distribution functions we classify the spontaneous signals according to the coherence range. Rayleigh and hyper-Rayleigh scattering are shown to be short range coherent signals. The signal dependence on wave vector, number of molecules and molecular density is discussed for molecular and polymer solutes. Several two-photon induced signals: second harmonic generation, hyper-Rayleigh scattering, two photon fluorescence and hyper-Raman are described within the same framework.

1 Introduction

Nonlinear optical signals are generated by the interaction of a material system with several laser beams. There are different types of signal classifications: spontaneous vs. stimulated, coherent vs. incoherent, short vs. long range. Some signals scale like $\sim N$ are others like $\sim N^2$ with the number of active molecules. The many types of signals are usually treated using different levels of formalisms, making it hard to precisely establish their connections and often confusing with esoteric acronyms (CARS, HORSES e.t.c.). The reason for such a baffling plethora of non-linear techniques is that they involve several interactions between the optical field and matter. Since both may be characterized by several parameters (transition dipole moments, energy levels, central frequencies, polarizations, arrival times etc.) we obtain many possible experimental setups. In this lecture we present a unified classification of these signals based on the last interaction that generate the signal field. This classification serves as a basis for a perturbative expansion, thus creating the diverse spectroscopic techniques.

The semiclassical theory of nonlinear spectroscopy which assumes a classical optical field interacting with a quantum matter has had a great success in describing coherent measurements [1, 2, 3, 4, 5, 6, 7, 8]. The signals are written in terms of response functions which cannot describe spontaneous processes. The response function [1] is a perturbative expansion of the polarization. The polarization is the coherent molecular response to the incoming fields. It is treated as a source in Maxwell generating the signal mode electric field. The perturbative expansion leads to various molecular pathways. Thus, the signal is an interference between the pathways making it hard to interpret. These difficulties and limitations can be mitigated by using fully quantum mechanical description of both optical field and matter [7, 8, 9, 10, 11, 12]. Presenting this formalism and itsapplications is the main subject of this presentation.

As an example we consider a set up where two beams of frequency ω_1 and ω_2 generate a signal with frequency $\sim \omega_1 + \omega_2$. Possible signals of this type are: sum frequency generation (SFG), hyper Raleigh scattering (HRS), two

[1] There are two types of tools commonly used to compute the nonlinear optical signals. The first uses nonlinear susceptibilities, conventionally represented by double sided Feynman diagrams for the density matrix. The second is given by Fermi Golden rule for molecular transitions from its initial to the final state and represented by single sided Feynman diagrams [6, 4, 1] for the wavefunction.

photon induced fluorescence (TPIF) and hyper Raman (HRA). Such signals are used for various spectroscopic applications for probing molecule energy levels and ultrafast dynamical processes as well as in high resolution imaging and nonlinear microscopy.

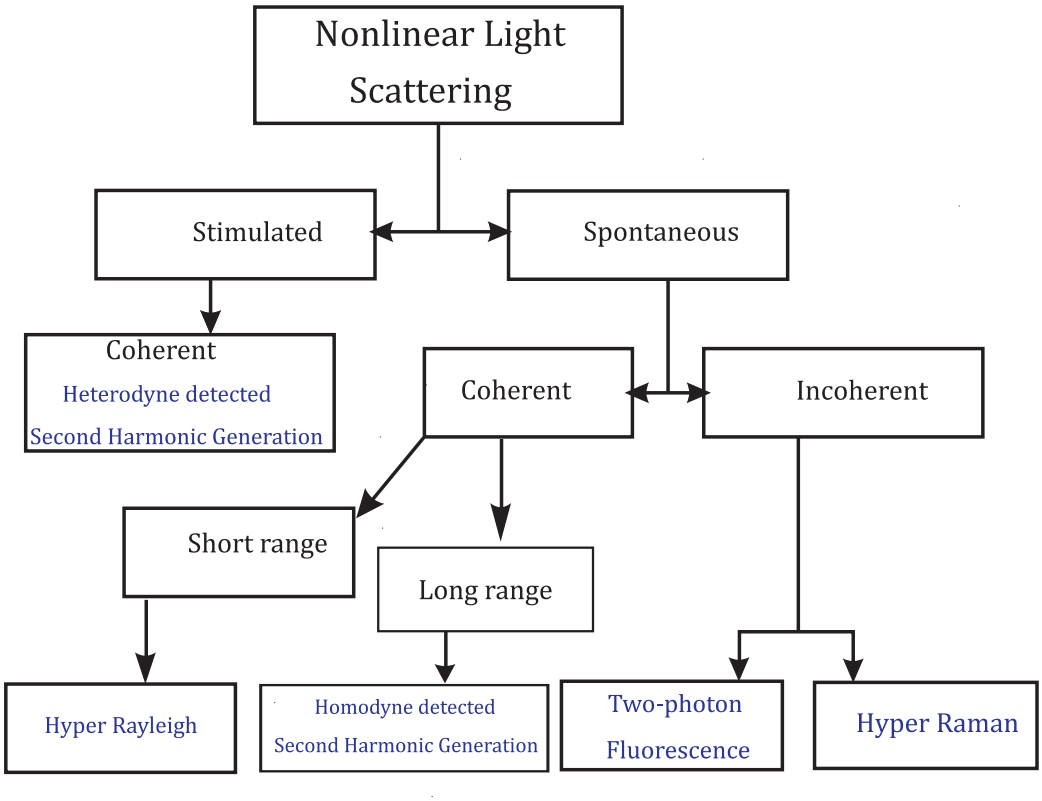

Figure 1: (Color on-line) Classification of various wave mixing signals.

SFG, TPIF, HRS are commonly used for biomolecular and cell imaging. Some studies had reported the simultaneous observation of two types of signals e.g. SFG+TPF and SFG+HRS in the same system [9, 10].

The different types of signals are depicted in Fig. 1. The primary classification is into stimulated (coherent) $S_{ST,coh}$ and spontaneous S_{SP}. The latter are divided into incoherent $S_{SP,inc}$, coherent short range $S_{SP,coh,sr}$ and long range $S_{SP,coh,lr}$. This gives for the total signal:

$$S = S_{ST,coh} + S_{SP,inc} + S_{SP,coh,sr} + S_{SP,coh,lr} \tag{1}$$

The optical signals are broadly classified as either stimulated where the signal is generated in the direction of an existing strong classical field, or spontaneous where the signal is generated in a new direction i.e. the detected mode is initially in the vacuum state. By treating the radiation field quantum mechanically we are able to describe both spontaneous and stimulated processes

The next layer of classification is into coherent, where the signal has a well defined phase with respect to the driving field, or incoherent where no such phase relation exists. Stimulated signals are coherent, scale as $\sim N$ and the field itself (both amplitude and phase) can be obtained by heterodyne detection. Spontaneous signals can be however either coherent or incoherent. The homodyne detected coherent signal generated in a sample much larger than the optical wavelength is directional, and scales as $\sim N^2$. However short range correlations can induce a Rayleigh (hyper Raleigh) scattering signal coming from pairs of closeby molecules. This signal is isotropic and scales as $\sim N$ [10] .

Spontaneous incoherent signals are generated by molecules which emit independently. They scale as $\sim N$ and will be denoted spontaneous light emission (SLE). Such signals may be further classified as either Raman (hyper Raman) or fluorescence.

The general classification shown in Fig. 1 holds to all orders in the fields. We shall recast the possible signals using compact superoperator expressions that can be expanded order by order in the optical fields to generate specific signals. To first order we only have the coherent linear response which is self heterodyned, or ordinary Raleigh scattering. The simplest model that shows all of these signals is depicted in Fig.2, where the emitted signals are either at or in the vicinity of $\omega_1+\omega_2$. For this model the stimulated/coherent heterodyne detected signal is sum frequency generation (SFG). The spontaneous/coherent/long range signal is homodyne detected SFG. The spontaneous/coherent/short range signal is known in this case as hyper Raleigh, and the spontaneous/incoherent signal is two-photon-induced light emission. The latter can further be classified as two-photon induced florescence and hyper Raman. The ratio of the two depends on the pure dephasing rate. This further separation is well documented [1] and will not be repeated here.

Two detection modes are commonly used: heterodyne and homodyne. In semiclassical approach to an $n+1$ wave mixing measurement, n incoming waves interact with a molecule to induce a polarization $\sim \langle V(\mathbf{r},t)\rangle_{\{n\}}$

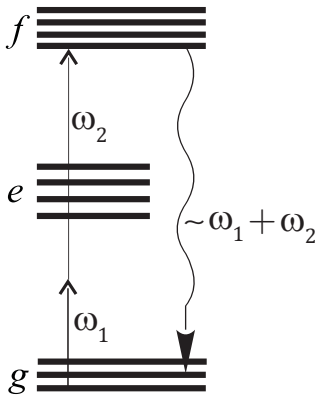

Figure 2: Level scheme for nonlinear two photon induced single photon emitted signals in the vicinity of $\omega_1 + \omega_2$.

(details andrationale for the notation will be provided in the next section). This polarization serves as a source in Maxwell's equations for the signal field $\mathcal{E}_{n+1}(\mathbf{r}, t)$ [11]. If necessary, the polarization can be further orientationally averaged and summed over all the molecules [3]. This is a simplified description. A more detailed analysis of the detection involves propagation effects (See Appendix A).

Heterodyne signals, detected by interference with a heterodyne mode, give both amplitude and phase of the nonlinear polarization. For a collection of N molecules, it is a coherent signal obtained by adding amplitude of all molecules and scales as $\sim \Im N \langle V(\mathbf{r}, t)\rangle_{\{n\}} \mathcal{E}^{\star}_{n+1}(\mathbf{r}, t)$. The heterodyne detected signal is phase sensitive and is directed along one of the possible 2^n phase matching directions $\Delta\mathbf{k} = \mathbf{k}_{\{n\}} - \mathbf{k}_{n+1} = 0$ $\mathbf{k}_{\{n\}} = \sum_{j=1}^{n} \pm\mathbf{k}_j$.

Homodyne detection is phase insensitive and measures the intensity of the scattered lighted $\sim |\langle V(\mathbf{r}, t)\rangle_{\{n\}}|^2$. It can be either coherent or incoherent. The later is a sum of individual molecular contributions $\sim N$, while the former is produced by molecular pairs and scales as $\sim N(N-1)$. The coherence length is related to the optical phase variation between two molecules $\Delta\mathbf{k}(\mathbf{r}_\alpha - \mathbf{r}_\beta)$. For a sufficiently large $\Delta\mathbf{k}$ the phase rapidly oscillates and the coherent part of the signal vanishes. The coherent molecular response thus shows up in the phase-matching direction $\Delta\mathbf{k} = 0$ and depends quadratically on the number of active molecules $\sim N^2$.

Inelastic processes, such as Hyper-Raman scattering are incoherent and

do not produce a macroscopic electric field. Different molecules emitl independently with random phases. One way to see this is by digressing from the semiclassical picture and looking at the joint state of the molecule and detected mode field ($|\texttt{mol,phot}\rangle$) at the end of the process: $|g,0\rangle+\alpha|g',1\rangle$ (See Fig. 2). This is a superposition of the inital state where the scattered mode is in the vacuum state with the molecule in state $|g\rangle$ and a state when the molecule is in the state $|g'\rangle$ with one emitted photon in the detected mode. The energy difference between the initial and final state of the molecule is supplied by the differnce between the incoming and the signal modes (in Fig. 2 it corresponds to $\omega_1+\omega_2-\omega_s$). The expectation value of the signal field mode (formally defined in Eq.(3)) with this state vanishes since $|g\rangle$ and $|g'\rangle$ are orthogonal.

In contrast, parametric or elastic scattering processes are always phase matched $\Delta\mathbf{k}=0$. A state like $|g,0\rangle+\alpha|g,1\rangle$ does give a finite field amplitude. At this level of theory Hyper-Rayleigh [12, 13, 14, 15] and Hyper-Raman [3, 16, 17, 10] scattering can be viewed as elastic and inelastic counterparts of two-photon induced fluorescence (i.e. incoherent and not phase matched).

The fully-microscopic description of the signals presented treats both the molecules and the optical field quantum mechanically. This allows to classify the signals according to the initial state of the detected mode rather than by the detection method. If that mode has initially a large number of photons one has a stimulated (emission or absorption), process. If it is in the vacuum state we have a spontaneous process. Stimulated processes, such as pump-probe, are heterodyne detected [11]. We shall mainly focus on spontaneous processes, but present the stimulated signals for completeness. Understanding the connection between the various signals is important for applications to nonlinear imaging [18, 19]. We show that the coherent part of the scattering should be classified according to the coherence range. Rayleigh and nonlinear light scattering are coherent processes involving pairs of molecules. However they only probe short range correlations and therefore scale as $\sim N$. When intermolecular interactions are important the density dependent part of the Rayleigh signal shows up. That component becomes dominant in the vicinity of anomalous first order phase transitions and vanishes for ordinary first order transitions in dilute solutions of molecules.

In the next section we calculate the signals using quantum-mechanical description of the field. We recast them into a form suitable for perturbative expansion. The non-equilibrium Green's functions, will be used. These can be represented graphically close time path loop diagrams CTPL [20].

Some signals scale with the single molecule and others with molecular pair distribution functions. The third section surveys statistical models for these distribution functions. For a solution of weakly interacting molecules or polymers signatures of structural phase transition are illustrated. The last section summarizes our results and presents a comparison of various two-photon-induced signals based on the level scheme in Fig. 2.

2 Spontaneous, stimulated, coherent and incoherent nonlinear wave mixing.

We shall partition the optical field into its positive and negative frequency components: $E(\mathbf{r},t)+E^{\dagger}(\mathbf{r},t)$. The positive frequency optical field mode operator at point $\mathbf{r}$ and time t is given by the sum of all optical modes (including the detected $n+1$ mode):

$$E(\mathbf{r},t)=\sum_{j=1}^{n+1}\sqrt{\frac{2\pi\omega_j}{\Omega}}a_j(t)\exp\left(i\left(\mathbf{k}_j\mathbf{r}-\omega_j t\right)\right) \tag{2}$$

Here, $a_j\left(a_j^{\dagger}\right)$ - are the annihilation (creation) operators for the j-the field mode, satisfying the bosonic commutation relation $\left[a_i,a_j^{\dagger}\right]=\delta_{i,j}$; Ω is the quantization volume.

The detector located at distance $|\mathbf{R}|$ from the sample (similar to the semiclassical case depicted in Fig. 5), sees a spherical wave:

$$E_{n+1}(\mathbf{R}+\mathbf{r},t)=\sqrt{\frac{2\pi\hbar\omega_{n+1}}{\Omega_{n+1}}}\times \tag{3}$$
$$\times a_{n+1}(t)\frac{\exp(i(\mathbf{k}_{n+1}(\mathbf{R}+\mathbf{r})-\omega_{n+1}t))}{|\mathbf{R}+\mathbf{r}|}$$

We shall eliminate the details of the detection geometry by defining the plane wave signal mode in a local system of coordinates $E_{n+1}(\mathbf{r},t)$ by Eq.(2). For a detector far from the sample we have:

$$E_{n+1}(\mathbf{R}+\mathbf{r},t)\approx E_{n+1}(\mathbf{r},t)\times\frac{\exp(i(\mathbf{k}_{n+1}\mathbf{R}))}{|\mathbf{R}|}$$

Henceforth we shall treat the signal mode as a plane wave. However spherical waves become important when the signals are calculated semi-classically via Maxwell's equations (See Appendix A).

We shall split the detected electric field into two terms: $E_{n+1}(\mathbf{r},t) = \mathcal{E}_s(r,t) + E_s(\mathbf{r},t)$. The classical (coherent) part $\mathcal{E}_s(\mathbf{r},t)$ is not affected by the interaction with matter, while $E_s(\mathbf{r},t)$ is initially ($t=-\infty$) in its vacuum state and changes its state due to the field/matter coupling. Following Ref. [21], the signal is defined as the change in the signal mode intensity due to the coupling with the system:

$$S(t) = S_{ST}(t) + S_{SP}(t) = \tag{4}$$
$$= \frac{\Omega}{2\pi\omega_s}\left[2\Re\int d\mathbf{r}\langle\mathcal{E}_s^{\star}E_s(\mathbf{r},t)\rangle + \int d\mathbf{r}\langle E_s^{\dagger}E_s(\mathbf{r},t)\rangle\right]$$

In order to calculate the expectation value of the optical field one must specify the total Hamiltonian of the field and matter:

$$H(t) = H_0 + H_{int}(t) \tag{5}$$

Here H_0 describes the sample and H_{int} stands for its interaction with the optical modes. We assume that the sample is made of N identical molecules with the positions $\mathbf{r}_\alpha$, energy levels $\{|i\rangle\}$ and transition dipole moments $\mu_{i,j}$. We shall partition the dipole operator into the excitation and de-excitation parts $V^{\dagger}(\mathbf{r}) + V(\mathbf{r})$, where:

$$V(\mathbf{r}) = \sum_{\alpha=1}^{N}\delta(\mathbf{r}-\mathbf{r}_\alpha)\sum_j\sum_{k>j}\mu_{jk}|j\rangle\langle k| \tag{6}$$

Using Eq.(2), Eq.(6), the radiation matter interaction in the Rotating Wave Approximation assumes the form:

$$H_{int}(t) = H_{int}^{(n+1)}(t) + H_{int}^{\{n\}}(t) = \tag{7}$$
$$= E_{n+1}(\mathbf{r},t)V^{\dagger}(\mathbf{r}) + E_{n+1}^{\dagger}(\mathbf{r},t)V(\mathbf{r}) +$$
$$+\sum_{j=1}^{n}E_j(\mathbf{r},t)V^{\dagger}(\mathbf{r}) + E_j^{\dagger}(\mathbf{r},t)V(\mathbf{r})$$

The stimulated and the spontaneous parts of the signal are given by the two terms in Eq.(4), which can be calculated by Heisenberg equations of motion

for the detected mode. For the stimulated part we have:

$$\frac{d}{dt}\langle \mathcal{E}_s^\star(\mathbf{r},t)E_s(\mathbf{r},t)\rangle = i\mathcal{E}_s^\star(\mathbf{r},t)\langle[H_{int},E_s(\mathbf{r},t)]\rangle = \tag{8}$$
$$= i\left(\frac{2\pi\omega_s}{\Omega}\right)\mathcal{E}_s^\star(\mathbf{r},t)\langle V(\mathbf{r},t)\rangle$$

Here we used the fact that the coherent part of the detected mode is not affected by the interaction with the molecules. $\langle\cdots\rangle$ denotes averaging over the radiation and matter degrees of freedom.

To carry out this calculation we introduce superoperators which facilitate the bookkeeping of the various interactions [20]. For an arbitrary operator A these are defined as "LEFT" or "RIGHT" type by the action on an operator X as:

$$A_L X = AX$$
$$A_R X = XA$$

We further define the transformed superoperators of "PLUS" and "MINUS" type:

$$A_- = \frac{1}{\sqrt{2}}\left(A_L - A_R\right)$$
$$A_+ = \frac{1}{\sqrt{2}}\left(A_L + A_R\right)$$

The interaction Hamiltonian (7) recast in the superoperator representation assumes the form: $\sqrt{2}H_{int,-} = E_L V_L^\dagger + E_L^\dagger V_L - V_R^\dagger E_R - V_R E_R^\dagger$, where, for brevity, we have suppressed the time and coordinate arguments of the superoperators.

The time evolution of the dipole superoperators may be calculated in the interaction picture using the bare molecule Hamiltonian as a reference:

$$\langle V_\nu(\mathbf{r},t)\rangle = \mathtt{Tr}\left[V_\nu(\mathbf{r},t)\rho(t)\right] = \tag{9}$$
$$= \langle\left[\mathsf{e}^{i\left(H_{0,L}-H_{0,R}\right)t}V(\mathbf{r})\mathsf{e}^{-i\left(H_{0,L}-H_{0,R}\right)t}\right]_\nu\rangle =$$
$$= \langle\mathcal{T}V_\nu(\mathbf{r},t)\exp\left(-i\sqrt{2}\int_{-\infty}^{t}d\tau\int d\mathbf{r}' H_{int,-}(\tau,\mathbf{r}')\right)\rangle$$

Here the subscript ν stands either for L or R superoperator indices. $\mathcal{T}$ is the time ordering operator in Liouville space which when acts on a product of the following superoperators it rearranges them so that their time arguments increase from right to left.

Heterodyne detected $(n+1)$-wave mixing signals in a macroscopic ($N \gg 1$) sample are generated along one of the 2^n directions given by combinations of the n incoming wave vectors $\mathbf{k}_{\{n\}} = \pm\mathbf{k}_1 \pm \mathbf{k}_2 \cdots \pm \mathbf{k}_n$. This can be obtained by expanding Eq.(9) to first order in the n incoming modes each interacting once with a single molecule, and summing over all the molecules in the sample:

$$\langle V(\mathbf{r},t)\rangle_{\{n\}} = \sum_{\alpha=1}^{N} \delta\left(\mathbf{r}-\mathbf{r}_\alpha\right) \langle V_L(t)\rangle_{\{n\}} \mathtt{e}^{i\mathbf{k}_{\{n\}}\mathbf{r}} \tag{10}$$

The subscript $\{n\}$ signifies that the averaging involves the density operator calculated by taking into account interactions of each of incoming modes with a single molecule. The $n+1$ (signal) mode is treated separately.

When Eq.(8) together with the initial condition $\langle E_s(\mathbf{r}, t=-\infty)\rangle = 0$ and the expansion (10) are substituted into Eq.(4) we obtain the stimulated incoherent signal:

$$S^{(n)}_{ST}(t) = \mathtt{Im}\ F_1(\Delta\mathbf{k}) \int_{-\infty}^{t} d\tau \mathcal{E}^{\star}_s(\tau) \langle V_L(\tau)\rangle_{\{n\}} \tag{11}$$

where the auxiliary function $F_1(\Delta\mathbf{k}) = \sum_\alpha \mathtt{e}^{i\Delta\mathbf{k}\mathbf{r}_\alpha}$ carries all information about the macroscopic sample geometry as well as the distribution of molecules. It gives rise to phase matching, which is a hallmark of heterodyne detected signals. Self-heterodyne signals such as pump-probe [21, 11], and stimulated Raman/Hyper-Raman scattering also fall into the stimulated signal category.

We next turn to the spontaneous part of the signal (4). This is obtained by solving the Heisenberg equation of motion:

$$\begin{aligned} \frac{d}{dt}\langle E^{\dagger}_s(\mathbf{r},t) E_s(\mathbf{r},t)\rangle &= i\langle\left[H_{int}, E^{\dagger}_s(\mathbf{r},t)E_s(\mathbf{r},t)\right]\rangle = \\ &= 2\Im\left(\frac{2\pi\omega_s}{\Omega}\right)\langle E^{\dagger}_s(\mathbf{r},t) V(\mathbf{r},t)\rangle \end{aligned} \tag{12}$$

with the initial condition $\langle E_s^\dagger E_s\rangle(t=-\infty)=0$. The right hand side of this equation can be factorized provided the density operator is treated perturbatively with respect to the E_s part of the signal mode. To first order the spontaneous signal assumes the form:

$$S_{SP}^{(n)}(t)=2\mathtt{Re}\int d\mathbf{r}\int d\mathbf{r}' e^{i\mathbf{k}_{n+1}(\mathbf{r}-\mathbf{r}')}\times \tag{13}$$
$$\times\int_{-\infty}^{t}d\tau\int_{-\infty}^{\tau}d\tau' e^{i\omega_{n+1}(\tau-\tau')}\langle\mathcal{T}V_L(\mathbf{r},\tau)V_R^\dagger(\mathbf{r}',\tau')\rangle_{\{n\}}$$

When all interactions with the optical fields occur with the same molecule $\langle\mathcal{T}V_L(\mathbf{r},\tau)V_R^\dagger(\mathbf{r}',\tau')\rangle_{\{n\}}$ assumes the form $\langle\mathcal{T}V_L(\mathbf{r},\tau)V_R^\dagger(\mathbf{r}',\tau')\rangle_{\{n\}}\delta\left(\mathbf{r}-\mathbf{r}'\right)$ and we recover the incoherent signal (13). Expanding it to first order in the interactions with each of the incoming modes we obtain:

$$S_{SP,incoh}^{(n)}(t)=2\mathtt{Re}F_1(0)\int_{-\infty}^{t}d\tau\int_{-\infty}^{\tau}d\tau'\mathtt{e}^{i\omega_{n+1}(\tau-\tau')}\langle\mathcal{T}V_L(\tau)V_R^\dagger(\tau')\rangle_{\{n\}} \tag{14}$$

The incoherent ($F_1(0)=N$) homodyne detected signal is phase insensitive. n photon induced Fluorescence, Hyper-Raman scattering are examples of such signals.

The coherent part of the spontaneous signal is generated when the optical modes are allowed to interact with all possible molecular pairs in the sample. Interactions with different molecules are not time ordered and $\langle\mathcal{T}V_L(\mathbf{r},\tau)V_R^\dagger(\mathbf{r}',\tau')\rangle$ can be factorized into $\langle V_L(\mathbf{r},\tau)\rangle\langle V_R^\dagger(\mathbf{r}',\tau')\rangle$. By expanding the two factors to first order in each of the n incoming modes we obtain the coherent part of the homodyne detected signal:

$$S_{SP,coh}^{(n)}(t)=\mathtt{Re}\ F_2(\Delta\mathbf{k})|\int_{-\infty}^{t}d\tau e^{i\omega_{n+1}\tau}\langle V_L(\tau)\rangle_{\{n\}}|^2 \tag{15}$$

Here we have used the identity:

$$\int_{-\infty}^{t}d\tau\int_{-\infty}^{\tau}d\tau'=\frac{1}{2}\int_{-\infty}^{t}d\tau\int_{-\infty}^{t}d\tau'$$

The auxiliary function $F_2(\Delta\mathbf{k}) = \sum_{\alpha}\sum_{\beta\neq\alpha} e^{i\Delta\mathbf{k}(\mathbf{r}_\alpha-\mathbf{r}_\beta)}$ is determined by the distribution function of molecular pairs and the sample geometry. Eq.(15) describes for example n-harmonic generation and Hyper-Rayleigh scattering.

Eqs. (11), (14), (15) constitute the starting formal expressions for signals. Specific signals will be calculated in Section 4. In the next section we focus on the molecular and molecular pair distribution functions: $F_1(\Delta\mathbf{k})$, $F_2(\Delta\mathbf{k})$.

3 $n+1$ wave mixing in fluids and polymer solutions. The role of molecular distributions.

We now examine more closely the role of molecular distributions in nonlinear wave scattering. Following Ref. [22] we shall consider a system of N identical hard spheres molecules in a solvent whose diameter a is smaller than the wavelength λ_{n+1} of the detected mode. The molecules are placed in a solvent and occupy the volume $L^3 \approx \Omega'$. Eqs. (11), (14), (15) describe the scattering due to the solute. Three cases will be considered. First, we will look at the scattering from an ideal solute with no long range order as depicted in Fig. 3(c). Second we investigate the scattering from a solution of polymer molecules [23] (See Fig. 3(d)). Finally we discuss a real solution close to a phase transition point. This will be discussed in view of classification illustrated in Fig. 1.

For large samples $L|\Delta\mathbf{k}| \gg 1$. Recall that in the opposite limit the problem can be treated in the continuum limit, where Maxwell equations self-consistently connect the polarization $\langle V(\mathbf{r},t)\rangle_{\{n\}}$ and the induced electric field $E_{n+1}(\mathbf{r},t)$. In the latter case the signal is calculated in two steps. First, the atoms act as the primary sources induce the field at the aperture [24]. This field serves as the secondary source and for the signal, which is calculated using the propagator formalism.

Here the opposite size limit. We shall assume that the phase $\Delta\mathbf{k}\cdot\mathbf{r}$ does not change appreciably within the sample $L|\Delta\mathbf{k}| \ll 1$. The sample can no loger be treated as a continous media. We argue that statistical molecular properties of the mater become important. For large samples both semiclassical and quantum approaches yield the same result as shown in Appendix A.

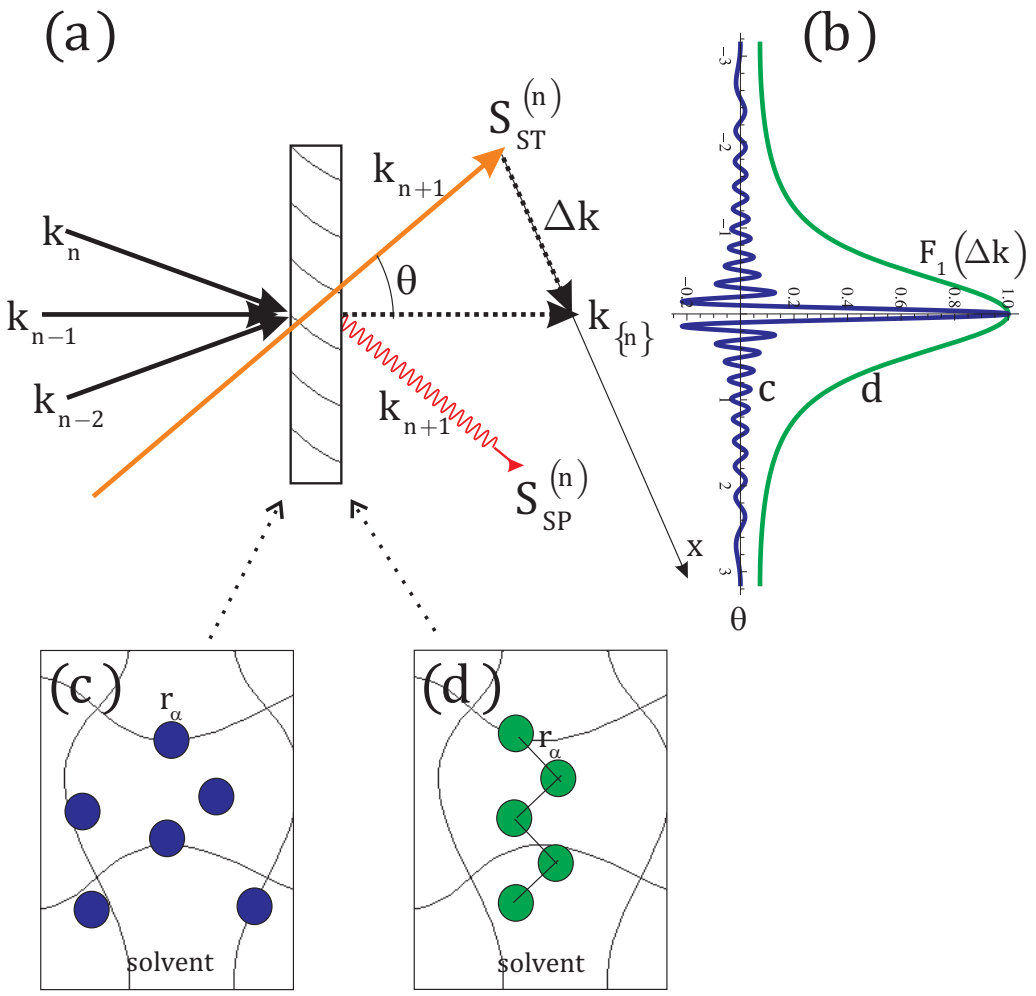

Figure 3: (Color on-line). (a) schematic of nonlinear wave mixing. θ is the phase matching angle between stimulated (red thick line)/spontaneous (wavy line) and a linear combination of the incoming modes (doted line). Panel (b) shows the angular distribution of the stimulated signal from a solute of noninteracting (blue rapidly oscillating curve) and polymer molecules (green smooth curve). Panels (c) and (d) represent a solute made of noninteracting and polymer molecules correspondingly. The parameters used are: $L/\lambda = 10$, $N = 100$, $b = 0.01$. $F_1(\Delta k)$ is shown normalized to the number of molecules.

3.1 Stimulated and Spontaneous incoherent signals.

Both signals described by Eqs. (11) and (14) are determined by the molecular distribution which is the subject of investigation in this subsection. The probability to find a solute molecule in the volume $d\mathbf{r}$ centered at $\mathbf{r}$ is given by $F_1(\mathbf{r})d\mathbf{r}/\Omega'$. The molecular distribution function is normalized so that its average value in the sample volume Ω' is the total number of molecules: $(N/\Omega')\int\limits_{\Omega'} F_1(\mathbf{r})d\mathbf{r} = N$. Converting the summation over a large number of independent molecular coordinates $\mathbf{r}_\alpha$ to an integration over $\mathbf{r}$ we obtain:

$$F_1(\Delta\mathbf{k}) = \frac{N}{\Omega'}\int\limits_{\Omega'} F_1(\mathbf{r})e^{i\Delta\mathbf{k}\cdot\mathbf{r}}d\mathbf{r} \tag{16}$$

More generally, the molecular distribution function must include internal molecular degrees of freedom and rotational averaging. These go beyond the scope of this presentation.

3.1.1 Ideal molecular solute. Fluids.

In the absence of long range order ($F_1(\mathbf{r}) = 1$, Fig.3(c)), assuming that $\Delta\mathbf{k}$ is along the $\hat{x}$ direction as shown in Fig.3(a), straightforward calculation of the integral (16) yields:

$$F_{1,fluid}(\Delta\mathbf{k}) = N\mathcal{P}_{fluid}(\theta) \tag{17}$$

with the polarization angular distribution:

$$\mathcal{P}_{fluid}(\theta) = \mathtt{sinc}(2\pi L\sin(\theta/2)/\lambda_{n+1})$$

Here λ is the wavelength; θ is the angle between detected $\mathbf{k}_{n+1}$ mode and a linear combination of the incoming modes $\mathbf{k}_{\{n\}}$.

3.1.2 A polymer solution.

We next turn to polymers (Fig.3(d)). The molecular probability distribution can be calculated using the theory of random walks model [25]:

$$\frac{N}{\Omega'}F_1(\mathbf{r})d\mathbf{r} = \frac{2}{N}\sum_j\sum_{i>j} W_{i,j}(r)d\mathbf{r} \tag{18}$$

$$W_{i,j}(r) = \left(\frac{3}{2\pi b^2\left(|i-j|\right)}\right)^{3/2}\exp\left(\frac{-3r^2}{2b^2\left(|i-j|\right)}\right) \tag{19}$$

Here the b constant depends on the polymer geometry $W_{i,j}(r)d\mathbf{r}$ is the probability of finding jth molecule at distance r from the ith molecule and in the volume element $d\mathbf{r}$. Converting the summation in Eq.(19) to an integration and substituting (18) into Eq.(16) we obtain:

$$F_{1,poly}(\Delta\mathbf{k}) = N\mathcal{P}_{poly}(\theta, N) \tag{20}$$
$$\mathcal{P}_{poly}(\theta, N) = \frac{2}{U(N,\theta)}\left[\mathsf{e}^{U(N,\theta)} - 1 + U(N,\theta)\right]$$
$$U(N,\theta) = \frac{8\pi^2}{3}\frac{b^2 N}{\lambda_{n+1}^2}\sin^2(\theta/2)$$

Equation (11) together with Eq.(17) or (20) give the stimulated signal, which is peaked in the direction $\Delta\mathbf{k} = 0$. Long-range order breaks the linear $\sim N$ dependence of the signal of ideal solutions.

3.2 Spontaneous coherent signals.

Spontaneous coherent signals given by Eq.(15) are determined by the Fourier transform of the molecular *pair* distribution function:

$$F_2(\Delta\mathbf{k}) = \frac{N(N-1)}{2\Omega'^2}\int\limits_{\Omega'}\int F_2(\mathbf{r}_\alpha, \mathbf{r}_\beta)\mathsf{e}^{i\Delta\mathbf{k}(\mathbf{r}_\alpha - \mathbf{r}_\beta)}d\mathbf{r}_\alpha d\mathbf{r}_\beta \tag{21}$$

Here $N(N-1)/2\Omega'^2 F_2(\mathbf{r}_\alpha, \mathbf{r}_\beta)d\mathbf{r}_\alpha\mathbf{r}_\beta$ is the joint probability of the molecules in the pair between $\mathbf{r}_\alpha, \mathbf{r}_\beta$ and $\mathbf{r}_\alpha + d\mathbf{r}_\alpha, \mathbf{r}_\beta + d\mathbf{r}_\beta$. The pair distribution function is normalized so that when integrated over the sample it gives the total number of molecular pairs:

$$\frac{N(N-1)}{2\Omega'^2}\int_{\Omega'}\int F_2(\mathbf{r}_\alpha, \mathbf{r}_\beta)d\mathbf{r}_\alpha d\mathbf{r}_\beta = \frac{N(N-1)}{2} \tag{22}$$

It can be partitioned as:

$$F_2(\mathbf{r}_\alpha, \mathbf{r}_\beta) = \lim_{|\mathbf{r}_{\alpha,\beta}|\to\infty} F_1(\mathbf{r}_\alpha)F_1(\mathbf{r}_\beta) + g_2(\mathbf{r}_\alpha, \mathbf{r}_\beta) \tag{23}$$

where $\mathbf{r}_{\alpha,\beta} = \mathbf{r}_\alpha - \mathbf{r}_\beta$. The interaction function g_2 measures the deviation of pair distribution function $F_2(\mathbf{r}_\alpha, \mathbf{r}_\beta)$ from a product of single molecule distributions $F_1(\mathbf{r}_\alpha)F_1(\mathbf{r}_\beta)$. It is a measure of the effect of intermolecular interactions.

3.2.1 Long range coherence.

The first term in Eq. (23) when substituted into Eq. (15) yields the long range coherent spontaneous signal:

$$F_2(\Delta\mathbf{k}) = N(N-1)\mathcal{P}^2_{fluid}(\theta) \tag{24}$$

Note that for linear scattering ($n = 1$), the signal (24) is indistinguishable from the incident beam. However the signal is distinct for nonlinear scattering with non-collinear beam geometry.

A similar result holds for a collection of N' polymers each made of N molecules. In the absence of long range order between the polymers, one can use Eq. (24), with $N \to N'N$; (See the neglected first term in Eq. (11) of Ref. [25]).

3.2.2 Short range coherence.

Short range coherent spontaneous signals described by Eq. (15). The distance between the molecules involved in the light-matter interaction is restricted by $g_2(\mathbf{r}_\alpha, \mathbf{r}_\beta)$, so that $r_{\alpha,\beta}/\lambda_{n+1} \ll 1$, the exponent in molecular pair distribution function (21) can be approximated by unity.

We start by considering a solution of hard sphere molecules of diameter a , the volume per solute molecule: $\pi a^3/6 = \Omega'/N = v$. In this case [26]:

$$g_2(\mathbf{r}_{\alpha,\beta}) = \begin{cases} 0, & r_{\alpha,\beta} > a \\ -1, & r_{\alpha,\beta} \leq a \end{cases} \tag{25}$$

Using the identity $\frac{1}{\Omega'}\int\int d\mathbf{r}_\alpha \mathbf{r}_\beta g_2(\mathbf{r}_\alpha, \mathbf{r}_\beta = \int d\mathbf{r}_{\alpha,\beta} g_2(r_{\alpha,\beta})$ we obtain:

$$F_{2,fluid}(\Delta\mathbf{k}) = -\frac{N-1}{2} \tag{26}$$

The short-range interaction for a collection of N' polymer molecules each comprised of N molecular segments has been calculated in Ref. [25]:

$$F_{2,poly}(\Delta\mathbf{k}) = \frac{N^4}{v'^2} X \mathcal{P}^2_{poly}(\theta, N) \tag{27}$$

where $v' = \Omega'/N'$ is the volume per single polymer molecule; X describe average short range interaction between the segments of two thread-like polymer molecules. Note that the first term in Eq. (13 (a)) of Ref. [25] corresponds

to the extra-short range coherent signal from the collection of the thread-like polymer molecules $\sim \frac{NN'}{\Omega'} F_{1,poly}(\Delta\mathbf{k})$. The coherence length is limited to a single polymer molecule.

To discuss the validity of the hard sphere model (26) we impose certain limitations on the solute molecules and their interactions. The solute is treated as non-ideal gas of classical molecules capable of undergoing a thermodynamic phase transitions. Second, the pair interaction potential falls off with the fourth or higher power of the distance. Third, the total potential energy of the system is representable as the sum of pair potentials which only depends only on the distance.

The deviation of the solute from the ideal gas is described by the fugacity Z normalized in density v^{-1} units:

$$Z = v^{-1} \exp\left(- \sum_{l \geq 1} \beta_l v^{-l} \right) \tag{28}$$

The irreducible integrals β_l are defined so that for the ideal gas $\beta_l \to 0$. We rewrite Eq.(28) in its differential form:

$$\frac{\partial \ln Z}{\partial \ln v} = \sum_{l \geq 1} l \beta_l v^{-l} - 1 \tag{29}$$

The pressure of the gas P above the solvent also shows the deviation from the ideal gas, which can be formally written with irreducible integrals as:

$$\left(\tfrac{\partial P}{\partial Z}\right)_T = \frac{NkT}{Zv} \tag{30}$$

$$\left(\tfrac{\partial P}{\partial \Omega'}\right)_T = -\frac{NkT}{\Omega'^2} \left(1 - \sum_{l \geq 1} l \beta_l v^{-l} \right) \tag{31}$$

where k is the Boltzmann constant and T is the temperature. Using the generalized form of the grand partition function (28), as well as connection between the cluster and irreducible integrals, it has been shown [26, 27] that:

$$\frac{1}{2\Omega'} \int g_2(\mathbf{r}_{\alpha,\beta}) d\mathbf{r}_{\alpha,\beta} = -\frac{Z^2 v^2}{2kT\Omega'} \left(\frac{\partial^2 P}{\partial^2 Z} \right)_T \tag{32}$$

Substituting Eq.(30) into Eq.(32) and utilizing Eq.(29) we obtain:

$$\frac{1}{2\Omega'}\int g_2(\mathbf{r}_{\alpha,\beta})d\mathbf{r}_{\alpha,\beta} = -\frac{v}{2\Omega'}\left(1-\frac{1}{1-\sum\limits_{l\geq 1} l\beta_l v^{-l}}\right) \tag{33}$$

Combining with Eqs. (23) and (21) we get:

$$F_{2,fluid}(\Delta\mathbf{k}) = -\frac{N-1}{2}\left(1-\frac{1}{1-\sum\limits_{l\geq 1} l\beta_l v^{-l}}\right) = \tag{34}$$

$$= -\frac{N-1}{2}(1-\frac{NkT}{\Omega'^2}\left(\frac{\partial P}{\partial\Omega'}\right)_T^{-1})$$

This equation confirms that the short range coherent spontaneous signal vanishes in an ideal solution. It also suggests that short range coherent signals from the solute in the absence of the strong Van-Der-Waals forces is not phase sensitive and depends on the solute density v^{-1}. Thus it represents Rayleigh ($n = 1$) and Hyper-Rayleigh ($n > 1$) scattering.

The first-principles calculation of the irreducible integrals β_l is a challenging task [27]. We only discuss the role of $\sum l\beta_l v^{-l}$. Phase transitions are characterized by divergence of the fugacity density series (28) on the real axis at $T = T_c$. Hence, $\sum l\beta_l v^{-l}$ either diverges (first order transitions) or becomes unity (anomalous first order transitions) [28, 29]. In the first case, at the singularity $\sum l\beta_l v^{-l}$ increases and reaches unity at some temperature T_0 lower than the temperature at which the singularity moves into the complex plane T_c. Close to T_0 the slight change in the partial volume of the solute dos not change with pressure and the second term in Eq.(34) dominates the short range coherent spontaneous signal.

An anomalous first-order transition occurs in the temperature range $T_o < T_a < T_c$. One can then neglect the second term in Eq.(34) and the signal reduces to those of the rigid spheres model (26). The $(N-1)/2$ factor signifies that only pairs of nearby molecules contribute to the short range coherence in this case.

4 Application to two-photon-induced signals.

In earlier sections we have presented a unified microscopic description of $n+1$ wave mixing processes. The nonlinear signal is defined as the change in the intensity of the detected mode due to the other n optical modes. The signal is formally expressed in terms of polarization superoperators which are calculated by the Heisenberg equations of motion for the field (stimulated signal) or the field intensity (spontaneous signal). We have identified four types of signals, which can be calculated by utilizing standard statistical quantities, namely the molecular and molecular pairs distribution functions. These results can be summarized as follows:

$$S^{(n)}(t) = S^{(n)}_{ST}(t) + S^{(n)}_{SP,icoh}(t) + S^{(n)}_{SP,coh,lr}(t) + S^{(n)}_{SP,coh,sr}(t) \tag{35}$$

$$S^{(n)}_{ST}(t) = \mathtt{Im}\ N \left\{ \begin{array}{c} \mathcal{P}_{fluid}(\theta) \\ \mathcal{P}_{poly}(\theta, N) \end{array} \right\} \int_{-\infty}^{t} d\tau \mathcal{E}^{\star}_{s}(\tau) \langle V_L(\tau) \rangle_{\{n\}} \tag{36}$$

$$S^{(n)}_{SP,incoh}(t) = 2\mathtt{Re}\ N \int_{-\infty}^{t} d\tau \int_{-\infty}^{\tau} d\tau' \mathtt{e}^{i\omega_{n+1}(\tau-\tau')} \langle \mathcal{T} V_L(\tau) V^{\dagger}_R(\tau') \rangle_{\{n\}} \tag{37}$$

$$S^{(n)}_{SP,coh,lr}(t) = N(N-1) |\mathcal{P}_{fluid}(\theta) \int_{-\infty}^{t} d\tau e^{i\omega_{n+1}\tau} \langle V_L(\tau) \rangle_{\{n\}}|^2 \tag{38}$$

$$S^{(n)}_{SP,coh,sr}(t) = \left\{ \begin{array}{c} -\frac{N-1}{2} \mathtt{Re} \left(1 - \left(1 - \sum_{l \geq 1} l \beta_l v^{-l} \right)^{-1} \right) \\ \frac{N^2}{v'} \mathcal{P}_{poly}(\theta, N) + \frac{N^4}{v'^2} X \mathcal{P}^2_{poly}(\theta, N) \end{array} \right\} \times \tag{39}$$

$$\times | \int_{-\infty}^{t} d\tau e^{i\omega_{n+1}\tau} \langle V_L(\tau) \rangle_{\{n\}}|^2$$

S_{ST} represents the stimulated heterodyne detected signal. This includes self-heterodyne detected techniques such as pump-probe and stimulated Hyper-Raman scattering. The remaining terms describe spontaneously generated signals which can be homodyne detected. $S_{SP,incoh}$ is incoherent, phase insensitive scales as $\sim N$ as for multi-photon induced fluorescence. $S_{SP,coh,lr}$ describes the coherent response of all possible molecular pairs. Linear signals of this type coincide with the incoming beam. Nonlinear signals include

Hyper-Raman scattering sum/difference frequency generation.

$S_{SP,coh,sr}$ is a short range coherent spontaneous signal. Identical oriented polymer molecules give a directed phase matched signal. The degree of phase-matching depends on the polymer size, internal structure and interaction between the polymers. The random-walk model suggests that the signal consists of two terms in the molecular density v'^{-1} expansion.

We have further investigated the nonlinear scattering from the solute represented by the non-ideal gas described by the osmotic pressure, density and fugacity. The signal is phase-insensitive and can be recast into an infinite series in the molecular density $\sum l\beta_l v^{-1}$. The exact calculation of the necessary irreducible integrals is a difficult challenge. We discussed two limiting cases of ordinary and anomaly first order transitions and compared them to the hard sphere model. Such signals are both phase-insensitive and depend on the molecular density and we associate them with Rayleigh and Hyper-Rayleigh scattering.

Eqs.(35) providea convinient starting point for the superoperator CTPL expansion of the nonlinear polarization. The rules are given in Appendix B. We shall illustrate this for stationary nonlinear spontaneous signals generated by two incoming classical fields: $\mathcal{E}_1 e^{-i\omega_1 t}$ and $\mathcal{E}_2 e^{-i\omega_2 t}$ around two-photon resonances $\omega_3 \approx \omega_1 + \omega_2$. The molecules are described by the three level ladder system: $\{\{|g\rangle, |g'\rangle\}, |e\rangle, |f\rangle\}$, shown in Fig. 4(B). The ground state manifold[2] contains at least two levels $\{|g\rangle, |g'\rangle\}$.

The incoherent signal (37) gives rise to hyper-Raman and two-photon induced fluorescence which may be distinguished by including dephasing processes [1]. This goes beyond the scope of this presentation.

Since all incoming modes are classical the stationary signals ($t \to \infty$) can be recast in terms of nonlinear susceptibilities using the CTPL shown in Fig. 4(C1) as:

$$S_{HRAM,TPIF}(-\omega_3;\omega_2,\omega_1) = \tag{40}$$
$$= 2N\mathtt{Re}\chi^{(5)}_{LR---}(-\omega_3;\omega_3,-\omega_2,\omega_2,-\omega_1,\omega_1)|\mathcal{E}_1|^2|\mathcal{E}_2|^2$$

[2]The model allows Brillouin scattering [30, 31]. That is the moving interference pattern, provided by the incoming pump fields and Stock shifted backward scattered generated wave, may create an acoustic wave. This, in turn, lifts the degeneracy of the molecular ground state and modifies the density dependent pre-factor for the short-range coherent signals. In some cases the acoustic wave may also reflect the incoming modes via Brag diffraction thus increasing the power of the generated signal. Brillouin scattering is a type of Raman scattering.

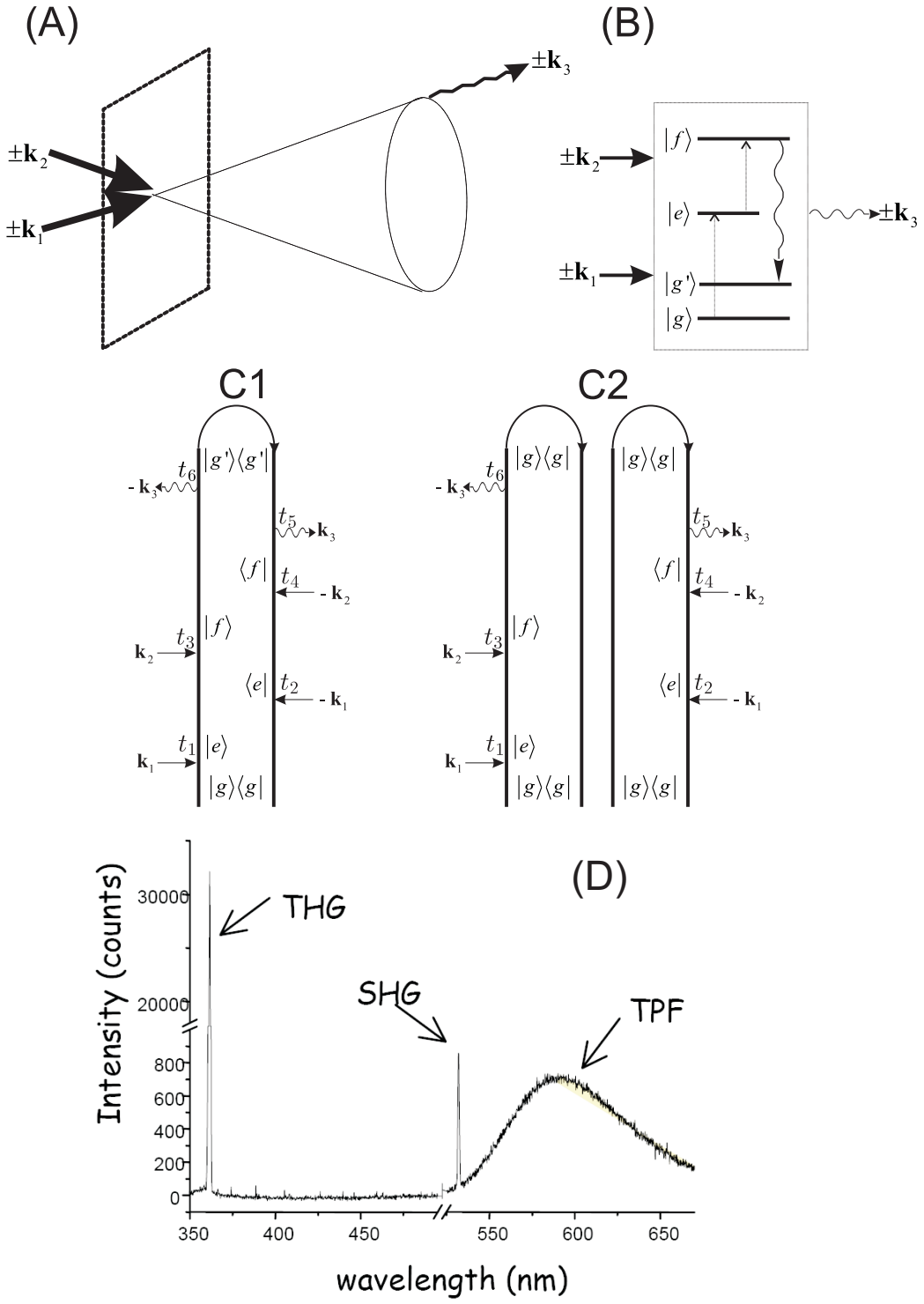

Figure 4: Three wave mixing process with two classical and one quantum modes: (A) phase-matching condition; (B) molecular level scheme; (C) CTPL for the incoherent Hyper-Raman and two-photon induced fluorescence (TPF) (C1) and long range coherent Homodyne detected sum frequency generation (SFG) as well as short range coherent Hyper-Rayleigh (C2). (D) specter measured from PMMA polymers of oriented DCM [18].

where the susceptibility is recast in the mixed representation (L/R for the generated mode, and $+,-$ for the classical incoming modes [20]). It can be written in terms of the Green's function $G(\omega) = \hbar/(\hbar\omega - H_0 + i\hbar\gamma)^{-1}$, where γ is a dephasing rate:

$$\chi^{(5)}_{LR---}(-\omega_3;\omega_3,-\omega_2,\omega_2,-\omega_1,\omega_1) = \tag{41}$$
$$= \frac{i^5}{5!\hbar^5}\sum_p \langle g|VG^\dagger(\omega_g+\omega_1)VG^\dagger(\omega_g+\omega_1+\omega_2)V^\dagger\times$$
$$\times G^\dagger(\omega_g+\omega_1+\omega_2-\omega_3)VG(\omega_g+\omega_1+\omega_2)V^\dagger G(\omega_g+\omega_1)V^\dagger|g\rangle$$

Here p stands for permutations of the incoming field within each branch of the loop diagram. Expanding Eq.(41) in molecular energy levels $\omega_{eg},\omega_{ef},\omega_{fg}$ and the corresponding transition dipole moments $\mu_{eg},\mu_{ef},\mu_{fg}$ we obtain:

$$\chi^{(5)}_{LR---}(-\omega_3;\omega_3,-\omega_2,\omega_2,-\omega_1,\omega_1) = \tag{42}$$
$$= \frac{i^5}{5!\hbar^5}\sum_p\sum_{g,g'}\frac{|\mu_{eg}\mu_{ef}\mu_{fg'}|^2}{[(\omega_1-\omega_{eg})^2+\gamma^2]\,[\omega_1+\omega_2-\omega_{fg}+i\gamma]}\times$$
$$\times\frac{1}{[\omega_1+\omega_2-\omega_{fg'}-i\gamma]\,[\omega_1+\omega_2-\omega_3-\omega_{gg'}-i\gamma]}$$

The long range coherent signal (38) for our model is a homodyne-detected sum frequency generation (SFG) [19, 32, 18]:

$$S_{SFG}(-\omega_3;\omega_2,\omega_1) = \tag{43}$$
$$= N(N-1)|\mathcal{E}_1|^2|\mathcal{E}_2|^2|\mathcal{P}_{fluid}(\theta)\delta(\omega_3-\omega_2-\omega_1)\chi^{(2)}_{L--}(-\omega_3;\omega_2,\omega_1)|^2$$

This susceptibility can be calculated from the CTPL in Fig.4(C2): (Ole-more to this equation)

$$\chi^{(2)}_{L--}(-\omega_3;\omega_2,\omega_1) = \sum_p\frac{i^2}{2!\hbar^2}\langle g|VG(\omega_g+\omega_1+\omega_2)V^\dagger G(\omega_g+\omega_1)V^\dagger|g\rangle =$$
$$= \sum_p\frac{i^2}{2!\hbar^2}\sum_g\frac{\mu_{ge}\mu_{ef}\mu_{fg}}{[\omega_1-\omega_{eg}+i\gamma]\,[\omega_1+\omega_2-\omega_{gf}=i\gamma]} \tag{44}$$

The short range coherent signal (39) for our model gives density dependent

hyper-Rayleigh (HRAY) scattering [33, 12, 13, 14]:

$$S_{HRAY}(-\omega_3;\omega_2,\omega_1)=\left\{\begin{array}{c} -\frac{N-1}{2}\mathtt{Re}\left(1-\left(1-\sum_{l\geq 1} l\beta_l v^{-l}\right)^{-1}\right) \\ \frac{N^2}{v'}\mathcal{P}_{poly}(\theta,N)+\frac{N^4}{v'^2}X\mathcal{P}^2_{poly}(\theta,N) \end{array}\right\}\times$$
$$\times|\mathcal{E}_1|^2|\mathcal{E}_2|^2|\delta(\omega_3-\omega_2-\omega_1)\chi^{(2)}_{L--}(-\omega_3;\omega_2,\omega_1)|^2 \qquad (45)$$

In Fig.4(D) we display the experimental spontaneously generated signal from a polymer solute [18]. The SFG signal has a sharp resonance, as expected from the delta function in Eq. (43), while the TPIF signal is broadened and covers the range of $\omega_{g',g}$ in accordance with Eq. (40). The hyper-Rayleigh signal (4) has the same resonance as SFG, since both are determined by the square of the second order susceptibility.

Note that all the signals discussed above are generated by classical incoming fields, and may be also calculated using standard susceptibility without invoking the CTPL formalism. The present microscopic treatment can predict signals generated by non-classical incoming modes [34, 35, 36]. Furthermore, even though in this paper we neglected the molecular orientational degrees of freedom, they play important role in distinguishing between SFG and HRAY processes. To take that into account we shall add a superscript to the transition dipole moment $\mu^i_{\alpha\beta}$ indicating its orientation with respect to the i-th component of the optical field. The intensity of (43) and (4) signals is then proportional to:

$$\langle(\mu^{i'}_{g'e'})^\star(\mu^{j'}_{e'f'})^\star(\mu^{k'}_{f'g'})^\star\mu^i_{ge}\mu^j_{ef}\mu^k_{fg}\rangle_{rav} \qquad (46)$$

where primed and unprimed indices denote two different molecules in the molecular pair; $\langle\cdots\rangle_{rav}$ is rotational averaging [33]. For such long range coherent signals such as SFG, correlation between the two molecules in the pair is negligible and Eq.(46) can be factorized as: $|\langle\mu^i_{ge}\mu^j_{ef}\mu^k_{fg}\rangle_{rav}|^2$. In an isotropic media, this vanishes by symmetry [10, 37] leaving only short range coherent signals HRAY.

5 Acknowledgments

This work was supported by the National Science Foundation Grant CHE-0745892 and National Institutes of Health Grant GM59230. We wish to thank Professor Paul Berman for useful discussions.

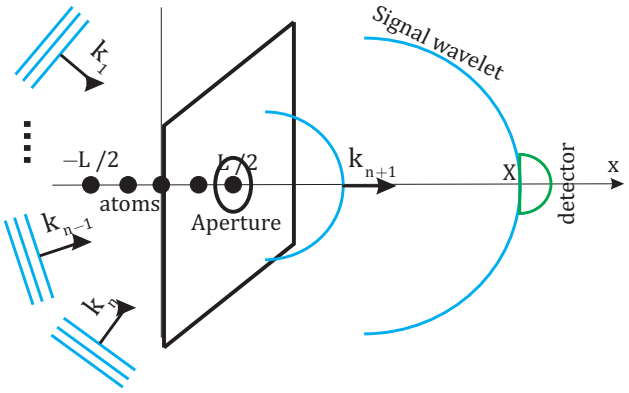

Figure 5: (Color on-line) Semi-classical heterodyne detection of incoherent nonlinear signals.

A Semiclassical vs. quantum field derivation of heterodyne detected signals.

In this appendix we calculate the heterodyne detected incoherent nonlinear signal from a linear chain of molecules which interact with $n+1$ classical optical fields. The chain extends between $-L/2$ to $L/2$ along the x axis. The heterodyne detected signal is given by the electric field of the signal mode at $x = X$ far from the sample, as shown in Fig.5. We shall demonstrate equivalence of the semiclassical and quantum approaches.

We start with the semiclassical of the signal field. Following Ref.[24] the calculation will be divided into two steps. We first derive the electric field on the auxiliary object (aperture) via Maxwell's equations with the optical field driven by the nonlinear polarization of the atomic *primary* sources. Second, the aperture serves as the point *secondary* source of a spherical signal wave which is calculated with the propagator formalism.

For $k_{\{n\}}L \gg 1$, the sample can be treated as continuous medium. The incoming waves create a nonlinear polarization wave along the sample:

$$P_{\{n\}}(x,t) = P_n(t) \exp\left(i\left(k_{\{n\}}x - \omega_{\{n\}}t\right)\right) \tag{47}$$

where $P_n(t)$ is slowly varying $|\frac{\partial}{\partial t}P_{\{n\}}(t)| \ll |\omega_{\{n\}}P_{\{n\}}(t)|$. This polarization is the primary source of the generated mode whose electric field is:

$$E_{n+1}(x,t) = \mathcal{E}_{n+1}(x,t) \exp\left(i(k_{n+1}x - \omega_{n+1}t)\right) \tag{48}$$

where $\mathcal{E}_{n+1}(t)$ is the slowly varying field amplitude (in space and time).

The electric field of the generated mode and the polarization induced by the incoming modes are connected by the Maxwell equations:

$$\left(\frac{\partial^2}{\partial x^2} + \left(\frac{k_{n+1}}{\omega_{n+1}}\right)^2 \frac{\partial^2}{\partial t^2}\right) E_{n+1}(x,t) = \tag{49}$$
$$= -\frac{4\pi}{c^2}\frac{\partial^2}{\partial t^2} P_{\{n\}}(x,t)$$

Substituting Eq. (47), (48) into (49) and using the slowly varying amplitude approximation for the generated and polarization we get:

$$ik_{n+1}\frac{\partial}{\partial x}\mathcal{E}_{n+1}(x,t) = \tag{50}$$
$$= -2\pi\frac{\omega_{\{n\}}^2}{c^2} P_{\{n\}}(t)\exp\left(i(\Delta k x - (\omega_{n+1} - \omega_{\{n\}})t)\right)$$

At the beginning of the illuminated region the amplitude of the generated mode vanishes $\mathcal{E}_{n+1}(-L/2,t) = 0$. Using this condition and integrating Eq. (50) over the sample range we obtain the generated mode at the aperture:

$$E_{n+1}(L/2,t) = -\frac{2\pi i\omega_{\{n\}}^2}{k_{n+1}c^2} P_{\{n\}}(t) L\,\mathtt{sinc}(\Delta k L/2)\times \tag{51}$$
$$\times \exp\left(i(k_{n+1}L/2 - \omega_{n+1}t)\right)$$

The signal field is given by Fresnel diffraction from a point-like secondary source which correspond to a single Huygens wavelet:

$$E_{n+1}(X,t) = \tag{52}$$
$$= -\frac{i}{k_{n+1}X} E_{n+1}(L/2,t)\exp\left(i(X - L/2)k_{n+1}\right) =$$
$$= -\frac{2\pi}{X n^2(\omega_n)} P_{\{n\}}(t) L\,\mathtt{sinc}(\Delta k L/2)\times$$
$$\times \exp\left(i(k_{n+1}X - \omega_{n+1}t)\right)$$

Here $n(\omega_{n+1})$ is the refractive index of the sample and the $1/X$ factor accounts for the spherical nature of the Huygens wavelet.

We now turn to the signal obtained from a quantum description of the field. Here each atom is the primary and only source of the signal wave. The

signal wave is given by the interference from the Huygens wavelets in Eq. (3). Using Eq. (7) one can obtain equation of motion for the photon annihilation operator:

$$\frac{d}{dt}a_{n+1}(t) = i\left[H_{int}^{(n+1)}, a_{n+1}(t)\right] = \tag{53}$$
$$= i\int dx\sqrt{\frac{2\pi\omega_{n+1}}{\Omega_{n+1}}}\langle V(x,t)\rangle_{\{n\}}\exp\left(-i(k_{n+1}x-\omega_{n+1}t)\right)$$

We shall integrate equation of motion (53) under the following conditions:

1. the expectation value of the polarization operator is given by Eq.(10);
2. initially the polarization $\langle V(x,-\infty)\rangle_{\{n\}}$ is zero;
3. the polarization has a slowly varying temporal amplitude:

$$\int_{-\infty}^{t}\langle V(\tau)\rangle_{\{n\}}d\tau = P_{\{n\}}(t)\frac{\exp\left(-i\omega_{\{n\}}t\right)}{-i\omega_{\{n\}}};$$

From Eq. (3) we obtain the signal optical field:

$$E_{n+1}(X,t) = \frac{-2N\pi\omega_{n+1}}{L\Omega_{n+1}\omega_{\{n\}}}\frac{(i(k_{n+1}X-\omega_{n+1}t))}{X}\times \tag{54}$$
$$\times P_{n+1}(t)\int_{-L/2}^{L/2}\exp\left(i\Delta kx\right)dx$$

Using the resonant condition $\omega_{n+1}-\omega_{\{n\}}\approx 0$, and Eq. (16), (17) we finally get:

$$E_{n+1}(X,t) = -\frac{2\pi N}{\Omega_{n+1}X}P_{\{n\}}(t)\mathtt{sinc}(\Delta kL/2)\times \tag{55}$$
$$\times\exp\left(i(k_{n+1}X-\omega_{n+1}t)\right)$$

By comparing Eq. (55) with (52) we see that the two approaches give identical results, apart from the factors $L/n'(\omega_{n+1})$ vs. N/Ω_{n+1} which are model

specific and arise from the single signal mode approximation. The heterodyne signal is obtained by treating the heterodyne wave as a spherical wave emitted by the aperture (which bring the Goui phase [24] factor $i/(k_{n+1}X)$): $\mathcal{E}_s(X,t) = i/(k_{n+1}X)\mathcal{E}_s(L,t)$ which brings up the Goui phase factor $i/(k_{n+1}X)$. Substituting the above equation along with Eq. (55)(or (52)) into the signal Eq. 4:

$$S_{HET} \sim \Im\langle V(\mathbf{r},t)\rangle_{\{n\}}\mathcal{E}^{\star}_{n+1}/X^2(\mathbf{r},t)$$

Formally we apply the Goui phase twice in Eq. 4 for propagating the signal and the heterodyne part. This leads to an overall pre-factor $1/(k_{n+1}X)^2$. One can skip the propagation steps and use Eq. (51) directly $E_{n+1} \sim iP_n$. This is the standard semiclassical procedure.

B Generalized susceptibility and it's CTPL representation.

In this appendix we introduce the generalized susceptibilities used in the last section. These are based on the superoperator non-equilibrium Green's functions (SNGF's) [38, 39]. The SNGF's of n^{th} order are defined as traces of time ordered products of such superoperators:

$$\langle \mathcal{T} A_+(t) \underbrace{A_+(t_n)\dots A_+(t_{n-m+1})}_{m} \underbrace{A_-(t_{m-n})\dots A_-(t_1)}_{n-m}\rangle$$

where $m = 0,\dots,n$. The SNGF's may contain an arbitrary number of $+$ and $-$ superoperators. The chronologically last superoperator must be a "+" one, otherwise the SNGF vanishes.

The material $\mathbb{V}$ and optical $\mathbb{E}$ SNGF's are defined as:

$$\mathbb{V}^{(n)}_{L\nu_n\dots\nu_1}(\tau,t_n,\dots,t_1) = \langle \mathcal{T} V'_L(\tau)V'_{\nu_n}(t_n)\dots V'_{\nu_1}(t_1)\rangle \tag{56}$$

$$\mathbb{E}^{(n)}_{\nu_n\dots\nu_1}(t_n,\dots,t_1) = \langle \mathcal{T} E'_{\bar{\nu}_n}(t_n)\dots E'_{\bar{\nu}_1}(t_1)\rangle \tag{57}$$

where subscript ν is the superoperator index which depends on the representation; $V'_\nu = V_\nu + V^\dagger_\nu$ and the net field operators. SNGF's of the form

$\mathbb{V}^{(m)}_{+\underbrace{-\ldots-}_{m}}$ give causal ordinary molecular response function of m^{th} order. The material SNGF of the form $\mathbb{V}^{(m)}_{+\underbrace{+\ldots+}_{m}}$ represent m^{th} moment of molecular fluctuations. The material SNGF of the form $\mathbb{V}^{(m)}_{+\underbrace{+\ldots+}_{m'}\underbrace{-\ldots-}_{m-m'}}$ indicates changes in m'^{th} moment of molecular fluctuations induced by $m-n$ light/matter interactions. In the other representation the material SNGF $\mathbb{V}^{(m)}_{L\underbrace{L\ldots L}_{n}\underbrace{R\ldots R}_{m-n}}$ represent a *Liouville space pathway* with $n+1$ interactions from the left (i.e. with the ket) and $m-n$ interactions from the right (i.e. with the bra).

The average material field in Eqs. (35)-(39) can be written in terms of the defined above SNGF's as:

$$\langle V_L(\tau)\rangle_{\{n\}} = \frac{i^n}{n!\hbar^n}\sum_{\nu_n}\ldots\sum_{\nu_1}\int_{-\infty}^{\infty} dt_n\ldots dt_1 \qquad (58)$$
$$\Theta(\tau)\mathbb{V}^{(n+1)}_{L\nu_n\ldots\nu_1}(\tau,t_n,\ldots,t_1)\times$$
$$\mathbb{E}^{(n)}_{\bar{\nu}_n\ldots\bar{\nu}_1}(t_n,\ldots,t_1)$$

where $t_n,\ldots,t_1$ are the incoming modes light/matter interaction times. The factor $\Theta(\tau)=\prod_{i=1}^{n}\theta(\tau-t_i)$ guarantees that the τ is the last light-matter interaction with the detected mode which has been taken care of separately. The indexes $\bar{\nu}_j$ are the conjugates to ν_j and are defined as follows: the conjugate of $+$ is $-$ and and the conjugate of L is R. Eq. (58) implies that is the excitation in the material are caused by fluctuations in the optical field and vice versa. Here we use a mixed representation in order to separate classical incoming ($\pm$ representation) and quantum detected (L,R representation) optical modes.

Eqs. (40), (43), (4) were obtained by recasting material SNGF's in Eq. (58) into the form of generalized susceptibilities. Those are formally defined as in

the frequency domain by performing a multiple Fourier transform:

$$\chi^{(n)}_{L\nu_n\ldots\nu_1}(-\omega_{n+1};\omega_n,\ldots,\omega_1) = \int_{-\infty}^{\infty} d\tau\ldots dt_1\Theta(\tau)e^{i(\omega_n t_n+\ldots+\omega_1 t_1)} \delta(-\omega_{n+1}+\omega_n+\ldots+\omega_1)\mathbb{V}^{(n)}_{L\nu_n\ldots\nu_1}(\tau,t_n,\ldots,t_1) \tag{59}$$

The SNGF $\chi^{(n)}_{+\underbrace{-\ldots-}_{n}}(-\omega_{n+1};\omega_n,\ldots,\omega_1)$ (with one + and the rest − indices) are the n^{th} order nonlinear susceptibilities or causal response functions. Others can be interpreted similarly to their time domain counterparts (56).

The generalized susceptibilities written in terms of L, R superoperators, can be represented by close-time path loop (CTPL) diagrams introduced by Schwinger-Keldysh many body theory. The following rules are used to construct the diagrams [21, 11]:

1. Time runs along the loop clockwise from bottom left to bottom right.

2. The left branch of the loop represents the "ket", the right represents the "bra".

3. Each interaction with a field mode is represented by an arrow line on either the right (R-operators) or the left (L-operators).

4. The field is marked by dressing the lines with arrows, where an arrow pointing to the right (left) represents the field annihilation (creation) operator $E_\alpha(t)$ ($E^\dagger_\alpha(t)$).

5. Within the RWA, each interaction with the field annihilates the photon $E_\alpha(t)$ and is accompanied by applying the operator $V^\dagger_\alpha(t)$, which leads to excitation of the state represented by ket and dexcitating of the state represented by the bra, respectively. Arrows pointing "inwards" (i.e. pointing to the right on the ket and to the left on the bra) consequently cause absorption of a photon by exciting the system, whereas arrows pointing "outwards" (i.e. pointing to the left on the bra and to the right on the ket) represent dexcitating the system by photon emission.

6. The observation time t, is fixed and is always the last. As a convention, it is chosen to occur from the left. This can always be achieved by a

reflection of all interactions through the center line between the ket and the bra, which corresponds to taking the complex conjugate of the original correlation function.

7. The loop translates into an alternating product of interactions (arrows) and periods of free evolutions (vertical solid lines) along the loop.

8. Since the loop time goes clockwise along the loop, periods of free evolution on the left branch amount to propagating forward in real time with the propagator give by the retarded Green's function G. Whereas evolution on the right branch corresponds to backward propagation (advanced Green's function $G^{\dagger}$).

9. The frequency arguments of the various propagators are cumulative, i.e. they are given by the sum of all "earlier" interactions along the loop. Additionally, the ground state frequency is added to all arguments of the propagators.

10. The Fourier transform of the time-domain propagators adds an additional factor of $i(-i)$ for each retarded (advanced) propagator.

11. The overall sign of the SNGF is given by $(-1)^{N_R}$, where N_R stands for the number of R superoperators.

References

[1] S. Mukamel. *Principles of nonlinear optical spectroscopy.* Oxford University Press New York, 1995.

[2] S. Mukamel and E. Hanamura. Four-wave mixing using partially coherent fields in systems with spatial correlations. *Phys. Rev. A*, 33:1099, 1986.

[3] D.L. Andrews and P. Allcock. *Optical harmonics in molecular systems.* Wiley-VCH Weinheim, 2002.

[4] R.J. Glauber. *Quantum Theory of Optical Coherence: Selected Papers and Lectures.* Wiley-VCH, 2007.

[5] MO Scully and MS Zubairy. *Quantum Optics*. Cambridge University Press, 1997.

[6] N. Bloembergen. *Nonlinear Optics*. World Scientific, 1996.

[7] W. Denk, JH Strickler, and WW Webb. Two-photon laser scanning fluorescence microscopy. *Science,*, 248(4951):73, 1990.

[8] J. Mertz. Nonlinear microscopy: new techniques and applications. *Current opinion in neurobiology*, 14(5):610–616, 2004.

[9] PD Maker. Spectral broadening of elastic second-harmonic light scattering in liquids. *Phys. Rev. A,*, 1(3):923, 1970.

[10] RW Terhune, PD Maker, and CM Savage. Measurements of nonlinear light scattering. *Physical Review Letters*, 14(17):681–684, 1965.

[11] C.A. Marx, U. Harbola, and S. Mukamel. Nonlinear optical spectroscopy of single, few, and many molecules: Nonequilibrium Greens function QED approach. *Phys. Rev. A,*, 77(2):22110, 2008.

[12] K. Clays and A. Persoons. Hyper-Rayleigh scattering in solution. *Phys. Rev. Lett.,*, 66(23):2980, 1991.

[13] G. Olbrechts, T. Munters, K. Clays, A. Persoons, O.K. Kim, and L.S. Choi. High-frequency demodulation of multi-photon fluorescence in hyper-Rayleigh scattering. *Optical Materials*, 12(2):221, 1999.

[14] M.C. Flipse, R. de Jonge, R.H. Woudenberg, A.W. Marsman, C.A. van Walree, and L.W. Jenneskens. The determination of first hyperpolarizabilities β using hyper-Rayleigh scattering: a caveat. *Chemical Physics Letters*, 245(2-3):297–303, 1995.

[15] A.S. Ranjini, P.K. Das, and P. Balaram. Binding Constant Measurement by Hyper-Rayleigh Scattering: Bilirubin- Human Serum Albumin Binding as a Case Study. *J. Phys. Chem. B*, 109:5950, 2005.

[16] S.J. Cyvin, J.E. Rauch, and J.C. Decius. Theory of hyper-Raman effects (nonlinear inelastic light scattering): selection rules and depolarization ratios for the second-order polarizability. *The Journal of Chemical Physics*, 43:4083, 1965.

[17] J.H. Christie and D.J. Lockwood. Selection Rules for Three-and Four-Photon Raman Interactions. *The Journal of Chemical Physics*, 54:1141, 1971.

[18] V. Le Floc'h, S. Brasselet, J.F. Roch, and J. Zyss. Monitoring of orientation in molecular ensembles by polarization sensitive nonlinear microscopy. *J. Phys. Chem. B*, 107(45):12403, 2003.

[19] M. Strupler, A.M. Pena, M. Hernest, P.L. Tharaux, J.L. Martin, E. Beaurepaire, and M.C. Schanne-Klein. Second harmonic imaging and scoring of collagen in fibrotic tissues. *Optics Express*, 15(7):4054–4065, 2007.

[20] O. Roslyak and S. Mukamel. A unified description of sum frequency generation, parametric down conversion and two-photon fluorescence. *Molecular Physics*, 107(3):265, 2009.

[21] O. Roslyak, C.A. Marx, and S. Mukamel. Generalized Kramers-Heisenberg expressions for stimulated Raman scattering and two-photon absorption. *Physical Review A*, 79(6):63827, 2009.

[22] B.H. Zimm. Molecular theory of the scattering of light in fluids. *The Journal of Chemical Physics*, 13:141, 1945.

[23] S. Mukamel. Solvation Effects on Four-Wave Mixing and Spontaneous Raman and Fluorescence Lineshapes of Polyatomic Molecules. *Adv. Chem. Phys.*, 70:165, 1988.

[24] N. Mertz. *Introduction to optical microscopy*. Roberts & Co, 2009.

[25] B.H. Zimm. The scattering of light and the radial distribution function of high polymer solutions. *The Journal of Chemical Physics*, 16:1093, 1948.

[26] B.H. Zimm. Application of the methods of molecular distribution to solutions of large molecules. *The Journal of Chemical Physics*, 14:164, 1946.

[27] J.E. Mayer and E. Montroll. Molecular distribution. *The Journal of Chemical Physics*, 9:2, 1941.

[28] J.E. Mayer and SF Harrison. Statistical mechanics of condensing systems. III. *The Journal of Chemical Physics*, 6:87, 1938.

[29] J.E. Mayer. Contribution to Statistical Mechanics. *The Journal of Chemical Physics*, 10:629, 1942.

[30] K. Brown, A.W. Brown, and B.G. Colpitts. Characterization of optical fibers for optimization of a Brillouin scattering based fiber optic sensor. *Optical Fiber Technology*, 11(2):131, 2005.

[31] Q. Lin, O.J. Painter, and G.P. Agrawal. Nonlinear optical phenomena in silicon waveguides: modeling and applications. *Optics Express*, 15(25):16604–16644, 2007.

[32] K. Komorowska, S. Brasselet, G. Dutier, I. Ledoux, J. Zyss, L. Poulsen, M. Jazdzyk, H.J. Egelhaaf, J. Gierschner, and M. Hanack. Nanometric scale investigation of the nonlinear efficiency of perhydrotriphenylene inclusion compounds. *Chemical Physics*, 318(1):12, 2005.

[33] K. Clays, E. Hendrickx, M. Triest, T. Verbiest, A. Persoons, C. Dehu, and J.L. Bredas. Nonlinear optical properties of proteins measured by hyper-Rayleigh scattering in solution. *Science*, 262(5138):1419, 1993.

[34] O. Roslyak and S. Mukamel. Photon entanglement signatures in difference-frequency-generation. *Optics express*, 17(2):1093–1106, 2009.

[35] O. Roslyak, C.A. Marx, and S. Mukamel. Nonlinear spectroscopy with entangled photons: Manipulating quantum pathways of matter. *Physical Review A*, 79(3):33832, 2009.

[36] O. Roslyak and S. Mukamel. Multidimensional pump-probe spectroscopy with entangled twin-photon states. *Physical Review A*, 79(6):63409, 2009.

[37] M. Kauranen, C. Boutton, T. Verbiest, M. N. Teerenstra, K. Clays, A. J. Schouten, R. J. M. Nolte, and A. Persoons. Supramolecular second-order nonlinearity of polymers with orientationally correlated chromophores. *Science*, 270:966, 1995.

[38] Adam E. Cohen and Shaul Mukamel. Resonant enhancement and dissipation in nonequilibrium van der waals forces. *Phys. Rev. Lett.*, 91:233202, 2003.

[39] Upendra Harbola and Shaul Mukamel. Superoperator nonequilibrium greens function theory of many-body systems; application to charge transfer and transport in open junctions. *Physics Reports*, 465:191, 2008.